Electronic Supplementary Material (ESI) for Journal of Materials Chemistry C.

Supporting Information of: "Molecular anchoring stabilizes low valence Ni(I)TPP on copper against thermally induced chemical changes".

Henning Maximilian Sturmeit,[1] Iulia Cojocariu,[2] Matteo Jugovac,[2,#] Albano Cossaro,[3] Alberto Verdini,[3] Luca Floreano,[3] Alessandro Sala,[3,4] Giovanni Comelli,[3,4] Stefania Moro,[4] Matus Stredansky,[3,4] Manuel Corva,[3,4] Erik Vesselli,[3,4] Peter Puschnig[5], Claus Michael Schneider[2,6], Vitaliy Feyer,[2,6,*] Giovanni Zamborlini,[1,*] and Mirko Cinchetti[1].

[1]*Technische Universität Dortmund, Experimentelle Physik VI, 44227 Dortmund, Germany.*

[2]*Peter Grünberg Institute (PGI-6), Forschungszentrum Jülich GmbH, Jülich, Germany*

[3] *CNR-IOM, Lab. TASC, s.s. 14 km 163,5, 34149 Trieste, Italy*

[4] *Physics Department, University of Trieste, 34127 Trieste, Italy*

[5]*Institut für Physik, Karl-Franzens-Universität Graz, NAWI Graz, 8010 Graz, Austria*

[6] *Fakultät f. Physik and Center for Nanointegration Duisburg-Essen (CENIDE), Universität Duisburg-Essen, 47048 Duisburg, Germany*

[#]*Present address: Istituto di Struttura della Materia-CNR (ISM-CNR), Trieste, 34149, Italy*

*Corresponding authors: v.feyer@fz-juelich.de, giovanni.zamborlini@tu-dortmund.de.

SI 1 - LEED

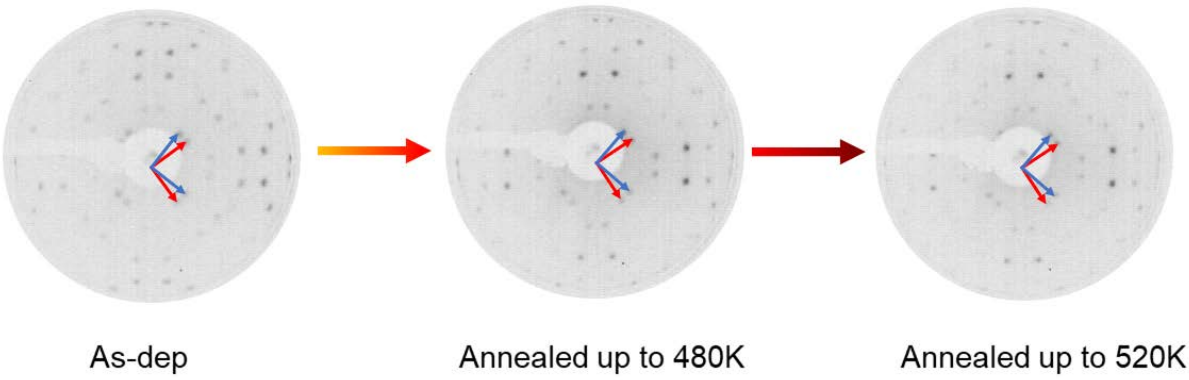

Figure 1S. LEED images taken at an electron kinetic energy of 20 eV, for the as-deposited NiTPP/Cu(100) interface and after annealing up to 480 and 520 K. The unit cell basis of the two mirrored domains are indicated by the blue and red vectors, respectively.

The superimposed lattice of the NiTPP molecule deposited on the Cu(100) surface, together with the resulting LEED pattern, can be described using the (4,3/-3,4) and (3,4/-4,3) matrices, as reported in Ref.[1] Upon annealing to 520 K, the diffraction pattern does not change, confirming that the unit cell of the NiTPP remains the same.

SI 2 – N 1*s* XPS

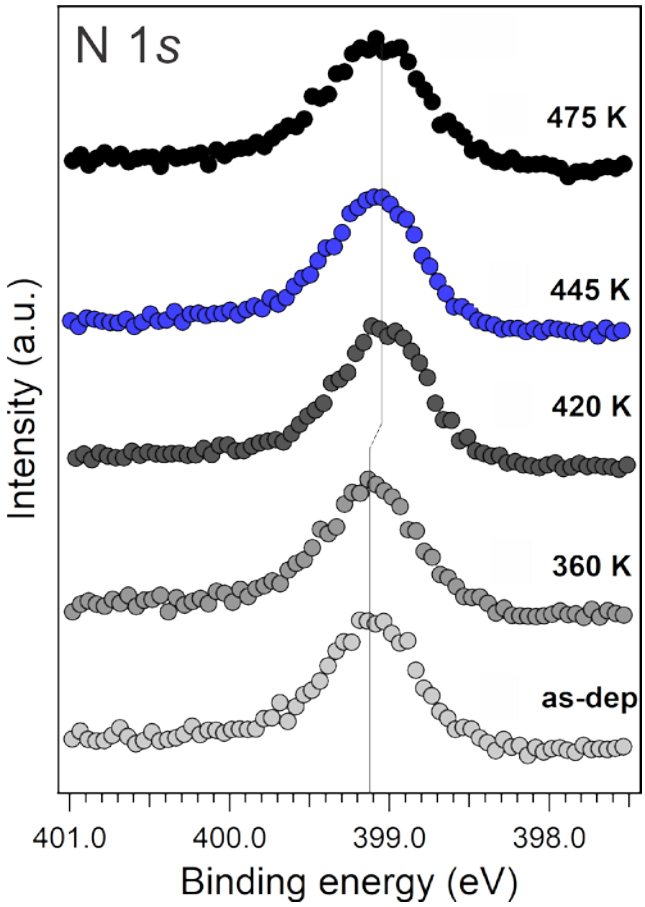

Figure 2S. N 1s XPS spectra of the NiTPP/Cu(100) interface taken after a stepwise annealing treatment up to 475 K. For each spectrum, the corresponding annealing temperature is indicated aside. All spectra were collected in normal emission geometry with a photon energy of 515 eV.

The nitrogen 1*s* core level spectrum was measured after a stepwise annealing to different temperatures (see Figure 2S) together with the C 1*s* described in the main text. While the as-deposited NiTPP molecule has four chemically inequivalent carbon species, the four nitrogen atoms in the macrocycle are equivalent. Therefore, the XPS spectrum shows only a single component at 399.1 eV. This indicates that the concentration of free-base porphyrins (H_2TPP) due to powder impurities is below our sensitivity. Upon annealing at 420 K, we only observed a small core level shift of the main line to lower binding energy (<-0.1 eV), while the overall line shape of the spectrum does not change, suggesting that the chemical environment experienced by the nitrogen atoms is similar to the one of the as-deposited NiTPP film. However, this cannot exclude the occurrence of the cyclodehydrogenation reaction since it was previously observed that the chemical modification of the macrocycle does not affect the N 1*s* core level.[2–4]

SI 3 – C 1*s* XPS at high temperatures

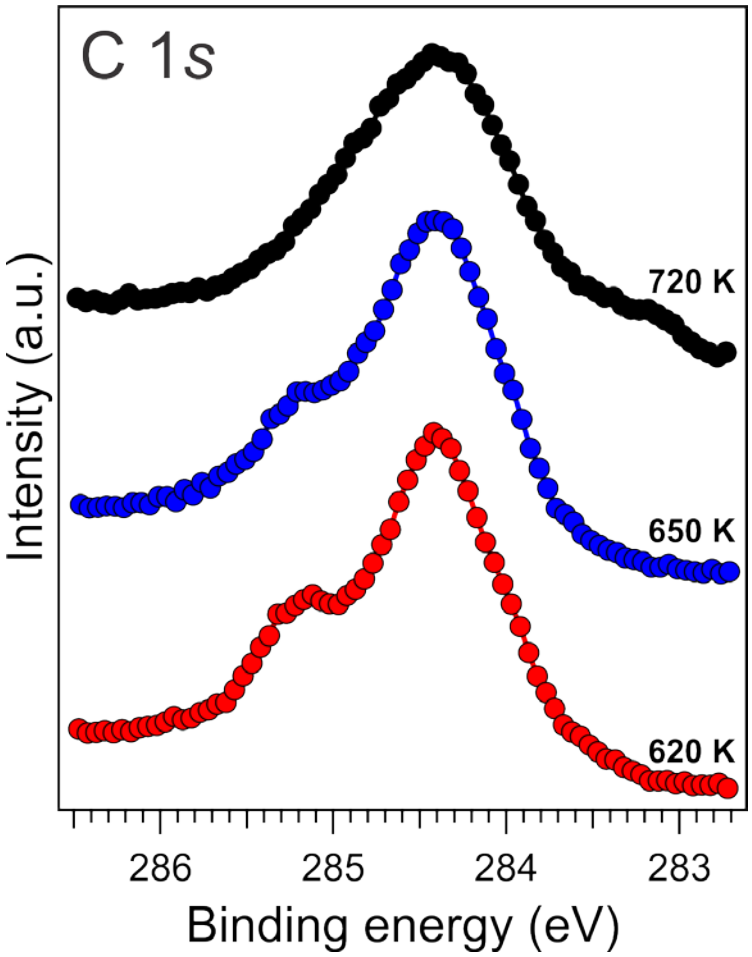

Figure 3S. C 1s XPS spectra of the NiTPP/Cu(100) interface taken after annealing, the corresponding temperature is indicated for each spectrum. The spectra are collected in normal emission geometry with a photon energy of 515 eV.

In order to follow the evolution of the chemical decomposition of the NiTPP layer, we collected X-ray photoemission spectra at the C 1*s* core level for higher annealing temperatures. The spectra were acquired with a photoemission electron microscope at the NanoESCA beamline. Up to 620 K, we do not observe any modification of the C 1*s* spectrum, while at 650 K its lineshape starts to change (see the high binding energy shoulder in Figure 3S, blue spectrum). At 720 K, we observe a very broad feature at 284.2 eV and another component growing on the low BE side. This is in agreement with the VB data described in the main text (Figure 3a), as at this temperature, the VB features related to the occupied molecular orbitals vanish, due to thermal decomposition of the NiTPP molecule.

SI 4 – DFT calculations

This section provides additional information about the procedure followed to obtain the simulated momentum maps displayed in Figure 3c of the main text. DFT calculations have been performed for the two molecules NiTPP (NiC44H28N4) and dh-NiTPP (NiC44H20N4) in the gas phase by employing the NWChem code.[5] The geometries of the molecules have been optimized using the Becke, 3-parameter, Lee-Yang-Parr (B3LYP) exchange-correlation functional[6,7] and the 6-31G* basis set. The calculations are performed for charge neutral and spin-unpolarized molecules. It should be noted that the appearance of the momentum space patterns of the frontier molecular orbitals to be presented below is quite robust against the basis set choice as well as the charge and spin state.

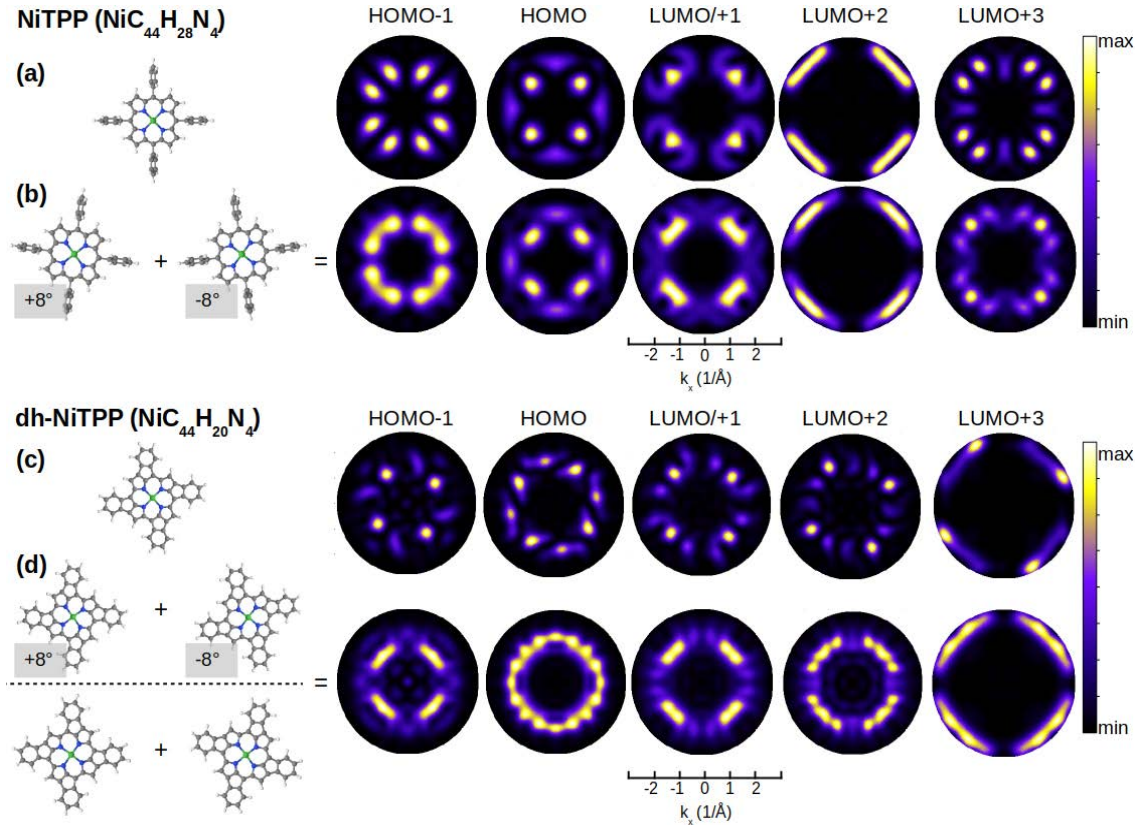

Figure 4S. Simulation of the momentum space pattern of the frontier molecular orbitals of NiTPP and dh-NiTPP. Panels (a) and (c) depict the Fourier transforms of the molecular orbitals for a single molecular orientation, while panel (b) and (d) take into account the azimuthal alignment of the molecule upon adsorption and the symmetry of the substrate as detailed in the text.

In Figure 4S, we compare the Fourier transforms of the frontier molecular orbitals of NiTPP and dh-NiTPP. Panel (a) shows a ball-and-stick model of the NiTPP molecule and the corresponding momentum maps, which are azimuthally oriented such that the N-Ni-N axis is at 45° to the k_x direction. To directly compare the simulated maps to the angle-resolved photoemission data, the different azimuthal orientation of the molecule for each domain must be taken into account, as already described in Ref.[1] In the present case, NiTPPs self-assemble in two mirrored domains (see

Fig. 1S) with the N-Ni-N axis oriented ± 8° with respect to the [100] direction of Cu(100), respectively. The resulting momentum maps are shown in panel (b).

The momentum patterns for the dehydrogenated molecule (dh-NiTPP) are displayed in panel (c). Here, the N-Ni-N axis of dh-NiTPP has the same orientation of the NiTPP one in panel (a). The resulting $|FT|^2$ of the dh-NiTPP frontier orbitals significantly differs from the ones of the NiTPP. In the case of the dh-NiTPP, we have to take into account that the molecule is chiral (see the ball-and-stick model in panel (c)), in order to compare the simulated and experimental momentum maps. Since the momentum maps are obtained averaging over a large surface area (several μm^2), we have to consider in the simulated momentum maps not only the azimuthal orientation of the molecule but also its chirality within the single domain. The results are reported in panel (d).

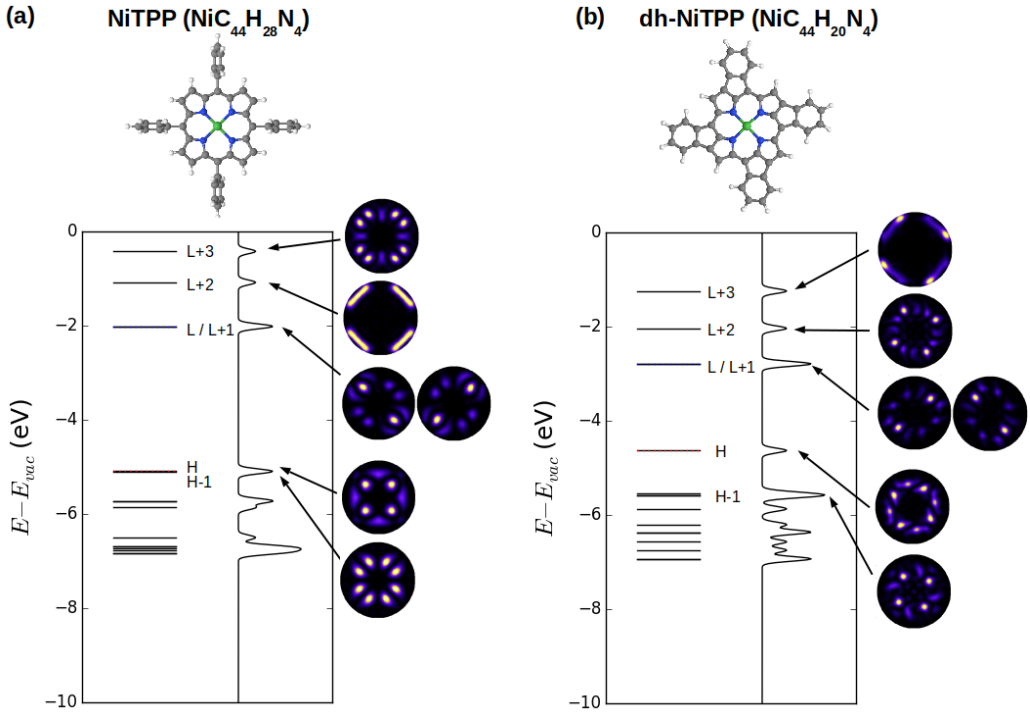

Figure 5S. Orbital energies and momentum maps (a) NiTPP and (b) dh-NiTPP from a gas phase DFT calculation with the B3LYP exchange-correlation functional. The momentum space patterns corresponding to the HOMO-1, HOMO, LUMO/LUMO+1, LUMO+2 and LUMO+3 orbitals are displayed next to the orbital energy diagram.

The comparison of the simulated momentum maps of the frontier molecular orbitals for NiTPP and dh-NiTPP molecules reveals pronounced differences. Since the shape of the measured momentum patterns does not change upon annealing, this provides strong evidence that the cyclodehydrogenation does not take place during the annealing. As depicted in Figure 5S, dh-NiTPP has a completely different electronic structure compared to NiTPP. This results in a completely different alignment of the frontier orbitals, resulting in a smaller HOMO-LUMO gap, and in π- to σ-symmetry change the LUMO+2 (whose filling up, in the NiTPP/Cu(100), is responsible for the +1 oxidation state of the Ni atom).[8]

SI 5 – Energy Barrier

The conversion percentage of phenyls in the new adsorption configuration, extracted from the C 1s XPS intensity peaked at 284.4 eV, as function of the temperature can be used to estimate the activation energy of the process (see the Figure below). Assuming a first order reaction, a simple Redhead analysis[9] yields a rough estimate of the reaction barrier of $0.25 \cdot T_{MaxRate} = 0.25 \cdot 400$ K = 100 ± 20 kJ/mol = 1.04 ± 0.21 eV. Where $T_{MaxRate}$ corresponds to the temperature value of the inflection point, estimated by deriving the conversion rate in first order.

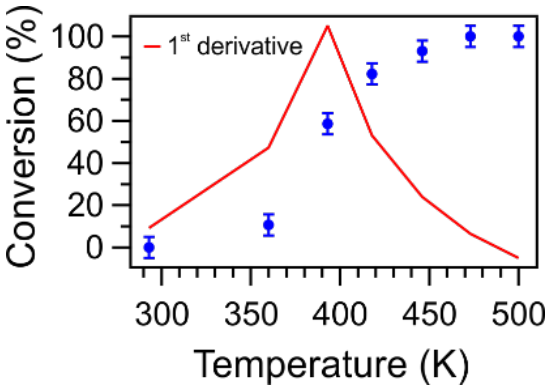

Figure 6S. The intensity of the XPS C 1s peak at 284.4 eV is plotted as a function of temperature (blue markers with error bars). The corresponding derivative is superimposed (full line, red) for better evaluation of the inflection point.

SI 6 – NEXAFS

The linear dichroism in the Ni L_3-edge NEXAFS spectra (see Fig. 7S) directly indicates the molecular nature of the orbitals participated by the Ni atoms, thus excluding the formation of Ni adatoms or NiCu alloying upon annealing, as due to transmetallation (see main text for details). In particular, the temperature transition, observed by STM intra-molecular topography and high resolution XPS of the C 1s peak, does not even affects the Ni NEXAFS resonances (either position or shape), which are the fingerprint of a nitrogen-coordinated Ni(I) ion in a tetrapyrrolic pocket.

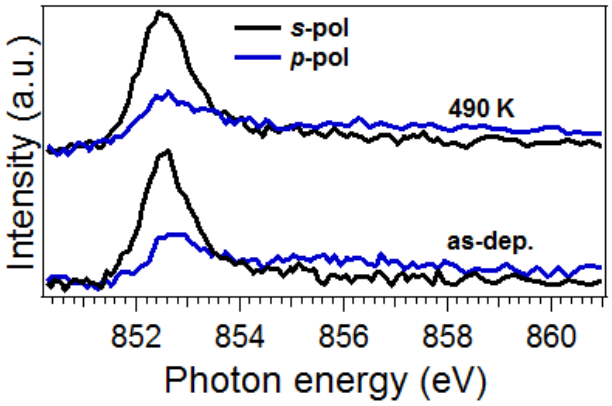

Figure 7S. Ni L_3-edge NEXAFS for the as-deposited NiTPP on Cu(100) surface (bottom panels) and after annealing up to 490 K (top panel), measured with s- and p-polarized light.

The average tilt-off angle of the different aromatic components of the NiTPP molecule can be probed by a NEXAFS investigation at the C and N K-edge. In the NEXAFS K-edge spectra, the intensity of electron transitions between the 1*s* core level and an unoccupied molecular orbital (MO) depends on the angle between the electric field of the linearly polarized incoming electromagnetic radiation and the spatial orientation of the unoccupied MOs. If the molecular layer owns a preferential orientation, the NEXAFS resonances measured with the electric field oriented parallel (s-polarization) and perpendicular (p-polarization) to the sample surface display different intensities, according to the symmetry of the involved MO. The comparison between the C K-edge NEXAFS spectra, measured with s- and p-polarized light, taken on the as-deposited and the annealed (up to 490 K) NiTPP film is shown in Figure 4b, in the main text.

Multiple electronic states contribute to the C K-edge:[10] the strong shoulder at ~284 eV is associated with the π* LUMO resonance localized on the carbon atoms of the tetra-pyrrolic macrocycle, the dominant peak at ~285.1 eV can be mainly attributed to the first π*-symmetry unoccupied MO localized on the carbon atoms of the phenyl rings. The higher energy resonances at ~287 and ~289 eV are again associated with π*-symmetry unoccupied MOs localized on the macrocycle and the phenyls, respectively. All these resonances display an accentuated polarization dependence (dichroism): the shoulder at 284 eV and the peak at 287 eV are maximum in p-pol and almost vanish in *s*-pol, indicating that the macrocycle is closely parallel to the surface and planar as well, as expected by the symmetric appearance of the molecules at STM. This experimental evidence is in full agreement with the corresponding NEXAFS

measurements at the N *K*-edge (shown in Figure 4a, in the main text), where the region below the ionization threshold is dominated by two π*-symmetry resonances displaying almost perfect dichroism. The carbon resonances at 285.1 and 289 eV displays an opposite polarization dependence indicating that the phenyl rings are rather oriented closer to the surface normal. After annealing, we could recognize the same NEXAFS resonances without significant energy shifts and with a similar dichroism trend, which indicates that both the macrocycle and the phenyls preserved their aromaticity. However, we observed an overall decrease of the phenyl resonance compared to the macrocycle ones (that is also decreasing but to a lower extent), which is accompanied by reduced dichroism pointing to a downward bending of the phenyls. A quantitative evaluation of the average tilt angle γ can be drawn from the intensity ratio of the NEXAFS resonance intensity in *s*- and *p*-pol, according to the relation $I_s/I_p \propto 1/2\ tg^2\gamma$, which applies to four-fold symmetry substrates.[11] The NEXAFS measured on the as-deposited film displays an intensity ratio of about 4:1 for the main phenyl resonance, which corresponds to an average phenyl tilt-off the surface by ~72˚±5˚. The determination of the phenyl resonance intensity ratio after annealing is more critical because of the lower intensity. However, we could estimate an average tilt-off angle of the phenyl of ~62˚±5˚ (*s*- to *p*-pol ratio of about 1.5:1).

The spectra for of the as-deposited and annealed NiTPP/Cu(100) system at the magic angle are reported in Fig. 8S, in order to disentangle the change of intensity of resonances due to reorientation of a specific moiety from the overall change of the electronic structure due to charge transfer. Assuming a 100% linearly polarized light, the spectrum at the magic angle can be obtained as a linear combination of the spectra taken in s- and p-pol configurations (magic angle= p-pol + 2·s-pol).[12] In Fig. 8S, the resonances associated with the phenyl rings display both an intensity decrease and an energy shift, whereas the macrocycle resonances remain unchanged upon annealing.

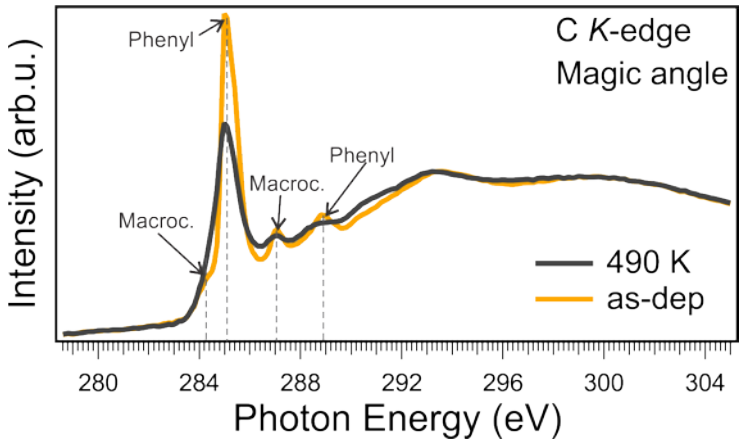

Figure 8S. C k-edge NEXAFS for the as-deposited NiTPP on Cu(100) surface (yellow curve) and after annealing up to 490 K (gray curve), at the magic angle. The main resonances are labelled according to their specific localization on the molecular moiety.

SI 7 – IR-Vis

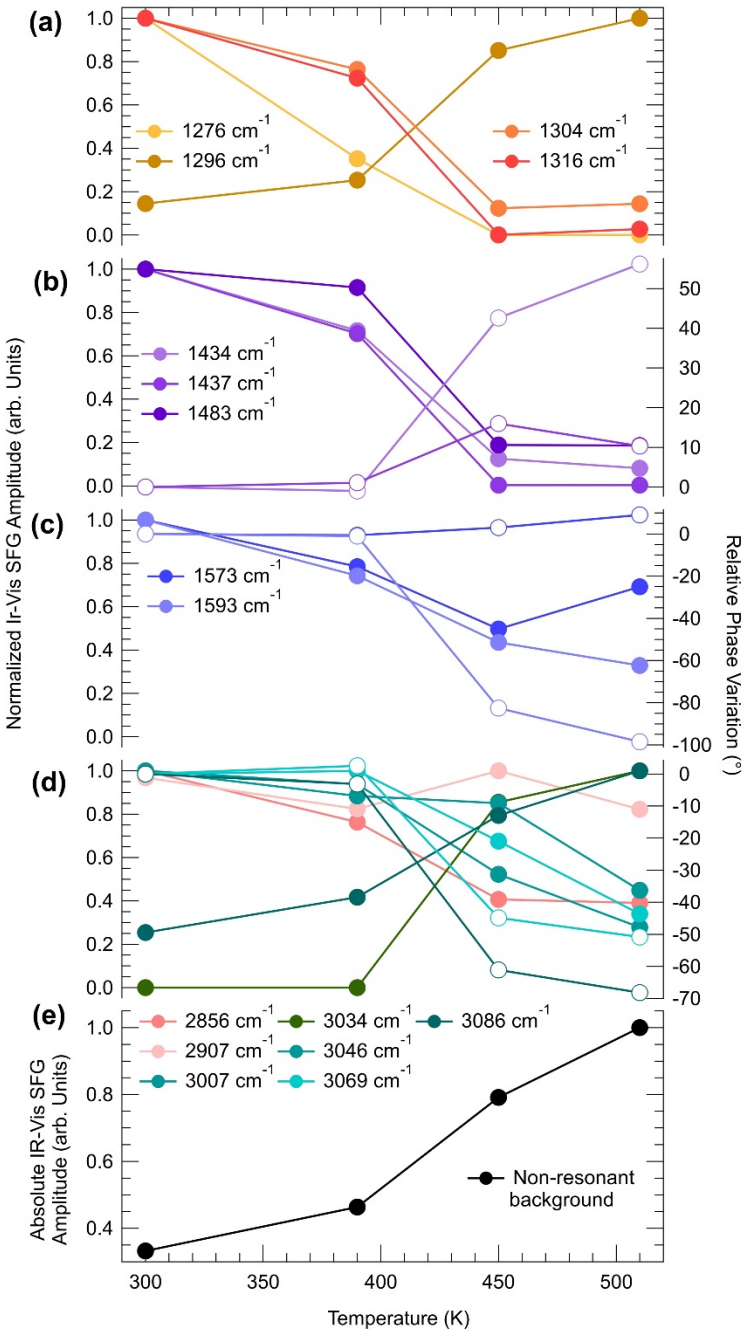

Figure 9S. Temperature evolution of the IR-Vis SFG lineshapes as obtained from the best fits of the data reported in Figure 4 according to the methods described in the text: (a-d) resonant amplitude (left scales, filled circles) and relative phase (right scales, empty circles); (e) amplitude of the non-resonant background. For better clarity, the color code of the resonances reflects the deconvolutions plotted in Figure 5.

This work			**Phenyl Modes** [13–15]		**Macrocycle Modes** [13–15]	
ω (cm^{-1})	*Δφ (°)*	*Γ (cm^{-1})*	*ω (cm^{-1})*	*Assignment*	*ω (cm^{-1})*	*Assignment*
1277	288	5	1269	δ(CH)	1269	ν(C_m-Ph), ν(NC_α)
1296	214	11	1283, 1285, 1289	Out-of-plane B_{1u}, A_{2u}, E_g		
1304	350	16			1302	ν(pyr half-ring), ν(NC_α), ν($C_\alpha C_\beta$)
1316	224	6	1317, 1318	Out-of-plane B_{1u}, A_{2u}	1313	ν(pyr quarter-ring)
1434	246-314	6	1438	Out-of-plane B_{1u}		
1437	97-113	6	1440	Out-of-plane A_{2u}		
1483	215	6	1470	δ(CCH), ν(CC)	1470, 1473, 1485	ν($C_\alpha C_m$)$_{sym}$, ν($C_\beta C_\beta$), ν(NC_α), ν($C_\alpha C_\beta$)
1573	105-114	3	1576, 1583, 1586	ν(CC), out-of-plane E_g, B_{1u}, A_{2u}	1572	ν($C_\beta C_\beta$), ν($C_\alpha C_m$), δ($C_\alpha C_m$)
1590-1593	139-238	4	1586	out-of-plane A_{2u}	1586, 1594	ν($C_\alpha C_m$)$_{sym}$, ν($C_\alpha C_m$)$_{asym}$, δ($C_\alpha C_m$Ph)
2856	280	14	3039, 3047, 3063, 3068, 3069, 3071, 3073, 3075	Symm. and asymm. ν(CH), out-of-plane E_g, B_{1u}, A_{2u}		
2907	295	21				
3007	87	8				
3033-3035	97	6				
3046	97	6				
3069	90-131	5				
3086	97-155	6				

Table 1S. Lineshape parameters obtained from the best fit and deconvolution procedure of the IR-Vis SFG data shown in Figure 5. The assignment of the observed vibronic modes to local coordinates and skeletal modes for 1.0 ML NiTPP/Cu(100) is obtained through comparison with previous literature data.[13–16] *The frequency and phase ranges indicated in the table account for the temperature-dependent evolution reported in Figure 6S.*

SI – Bibliography

1. Zamborlini, G. *et al.* Multi-orbital charge transfer at highly oriented organic/metal interfaces. *Nat. Commun.* **8**, 1–22 (2017).

2. Papageorgiou, A. C. *et al.* Self-terminating protocol for an interfacial complexation reaction in vacuo by metal-organic chemical vapor deposition. *ACS Nano* **7**, 4520–4526 (2013).

3. Xiao, J. *et al.* Temperature-dependent chemical and structural transformations from 2H-tetraphenylporphyrin to copper(II)-tetraphenylporphyrin on Cu(111). *J. Phys. Chem. C* **116**, 12275–12282 (2012).

4. Papageorgiou, A. C. *et al.* In Vacuo Porphyrin Metalation on Ag(111) via Chemical Vapor Deposition of Ru3(CO)12: Mechanistic Insights. *J. Phys. Chem. C* **120**, 8751–8758 (2016).

5. Valiev, M. *et al.* NWChem: A comprehensive and scalable open-source solution for large scale molecular simulations. *Comput. Phys. Commun.* **181**, 1477–1489 (2010).

6. Becke, A. D. Density-functional thermochemistry. III. The role of exact exchange. *J. Chem. Phys.* **98**, 5648–5652 (1993).

7. Chengteh Lee, Weitao Yang, and R. G. P. Development of the Colle-Salvetti correlation-energy formula into a functional of the electron density. *Phys. Rev. B* **37**, 785 (1988).

8. Zamborlini, G. *et al.* On-surface nickel porphyrin mimics the reactive center of an enzyme cofactor. *Chem. Commun.* 13423–13426 (2018). doi:10.1039/C8CC06739B

9. Redhead, P. A. Thermal desorption of gases. *Vacuum* **12**, 203–211 (1962).

10. Schmidt, N., Fink, R. & Hieringer, W. Assignment of near-edge x-ray absorption fine structure spectra of metalloporphyrins by means of time-dependent density-functional calculations. *J. Chem. Phys.* **133**, (2010).

11. Floreano, L. *et al.* Periodic arrays of Cu-Phthalocyanine chains on Au(110). *J. Phys. Chem. C* **112**, 10794–10802 (2008).

12. Stöhr, J. *NEXAFS Spectroscopy*. (Springer-Verlag Berlin Heidelberg, 1992). doi:10.1007/978-3-662-02853-7

13. Li, X. Y., Czernuszewicz, R. S., Kincaid, J. R., Su, Y. O. & Spiro, T. G. Consistent porphyrin force field. 1. Normal-mode analysis for nickel porphine and nickel tetraphenylporphine from resonance Raman and infrared spectra and isotope shifts. *J. Phys. Chem.* **94**, 31–47 (1990).

14. Rush, T. S. *et al.* Computational Modeling of Metalloporphyrin Structure and Vibrational Spectra: Porphyrin Ruffling in NiTPP. *J. Phys. Chem. B* **104**, 5020–5034 (2000).

15. Procyk, A. D. & Bocian, D. F. Vibrational Characteristics of Tetrapyrrolic Macrocycles. *Annu. Rev. Phys. Chem.* **43**, 465–496 (1992).

16. Scudiero, L., Barlow, D. E. & Hipps, K. W. Physical Properties and Metal Ion Specific Scanning Tunneling Microscopy Images of Metal(II) Tetraphenylporphyrins Deposited from Vapor onto Gold (111). *J. Phys. Chem. B* **104**, 11899–11905 (2000).